Significant features of ^{8}B scattering from ^{208}Pb at 170.3 MeV

R. S. Mackintosh*
Department of Physical Sciences, The Open University, Milton Keynes MK7 6AA, United Kingdom

D. Y. Pang†
School of Physics and Nuclear Energy Engineering, Beihang University, Beijing 100191, China and
International Research Center for Nuclei and Particles in the Cosmos, Beihang University, Beijing 100191, China
(Received 14 June 2013; published 18 July 2013)

The scattering of proton-halo nucleus ^{8}B from ^{208}Pb at 170.3 MeV is shown to reveal a distinctive pattern in the change in $|S_L|$ that is induced by coupling to breakup channels. The same pattern had been found for ^{8}B scattering from ^{58}Ni at 30 MeV, an energy near the Coulomb barrier, and has been linked to various other respects in which scattering for this proton-halo nucleus differs from that of other light, weakly bound nuclei. The increase in $|S_L|$ for $L < 80$, induced by breakup coupling, is associated with a substantial repulsive region in the dynamic polarization potential as determined by exact inversion. This repulsion appears to reduce the penetration of the projectile into the absorptive region of the interaction. This accounts for the fact that the increase in the total reaction cross section, due to breakup, is much less than the breakup cross section, and is consistent with the relatively small effect of breakup on the elastic scattering angular distribution compared with the large breakup cross section.

DOI: 10.1103/PhysRevC.88.014608 PACS number(s): 25.60.Gc, 24.50.+g, 24.10.Ht, 25.60.Bx

I. INTRODUCTION

Reference [1] presented elastic scattering angular distributions for ^{8}B scattering from ^{208}Pb at 170.3 MeV together with fits based on a folding model. In addition, CDCC calculations were presented that showed the effect on ^{8}B elastic scattering of coupling to proton plus ^{7}Be breakup channels. This is of particular interest because the scattering of candidate proton halo nucleus ^{8}B from ^{58}Ni at energies near the barrier shows features [2] which distinguish its scattering from that of other weakly bound light nuclei. One of these features emerges from a comparison of the change in $|S_L|$ that results from breakup of ^{8}B with the change in $|S_L|$ due to breakup coupling for ^{6}Li and ^{7}Be [3]. The quantity $|S_L|$ is the absolute value of S_L, the (diagonal) elastic scattering S matrix. Specifically, there is a different pattern according to which $|S_L|$ behaves the 'wrong way' (WW, see Ref. [4]), i.e., increases when the breakup channel coupling is included. The WW effect occurs in a wide range of channel coupling situations, and may well provide insight into the nonlocal effects that are commonly represented through a local dynamic polarization potential (DPP) [5]. Here we show that characteristic effects that have been found for ^{8}B at energies near the Coulomb barrier persist to much higher energies. This suggests that the other ways [2] in which the scattering of other weakly bound light nuclei differs from that of ^{8}B might occur over a wide energy range.

This work shows that the increase in total reaction cross section, that results from the coupling to breakup channels, is much less than the breakup cross section itself, thus linking the suppression of fusion to the specific nature of the DPP that we find.

*r.mackintosh@open.ac.uk
†dypang@buaa.edu.cn

II. THE BREAKUP CALCULATIONS

The continuum discretized coupled channels, CDCC calculations, see Ref. [6], were carried out with code FRESCO [7]. In these calculations the projectile ^{8}B is modeled as a valence proton in an $\ell = 1$ orbit about an inert ^{7}Be core. Both the proton and the ^{7}Be core were assumed to have spin zero. The proton-^{7}Be binding potential was taken to be of Woods-Saxon form with geometrical parameters $r_0 = 1.25$ fm ($R = 2.391$ fm) and $a = 0.65$ fm. The depth of this potential was adjusted to give the binding energy of a proton in the ground state of ^{8}B and was also used for the calculation of the continuum states. The proton-^{7}Be relative orbital angular momenta were included up to $\ell = 3$ with all couplings up to multipolarity $\lambda = 3$ (the multipole expansion of the coupling potential is defined in [6,7]). The continuum states were discretized up to a maximum proton-^{7}Be relative energy of $\epsilon_{\max} = 15.3$ MeV, corresponding to $k_{\max} = 0.8$ fm^{-1} in momentum space, with step size of $\Delta k = 0.1$ fm^{-1}. Convergence of the elastic scattering and breakup cross sections were verified by calculations with an increased model space with $k_{\max} = 1.0$ fm^{-1} and $\ell = 4$, $\lambda = 4$. The KD02 [8] nucleon-nucleus systematic potential was used for the proton-target optical potential at 21.3 MeV and the systematic single-folding nucleus-nucleus potential [9], evaluated at 148 MeV, was used for the ^{7}Be-target potential.

III. ESTABLISHING THE DYNAMIC POLARIZATION POTENTIALS

The dynamic polarization potential is calculated by performing $S_L \rightarrow V(r)$ inversion upon the S matrix produced by the CDCC calculation. The DPP is the result of subtracting the bare potential of the CDCC calculation from the inverted potential. The iterative-perturbative (IP) inversion procedure [10–12] produces a local potential that gives an essentially

exact reproduction of the input S_L, and therefore exactly reproduces the elastic scattering angular distribution from the CDCC calculation. Other forms of inversion exist that are more directly related to the wave function, and which do not precisely reproduce the elastic scattering angular distribution, see Ref. [12] for a discussion of this point.

The CDCC calculation treated the projectile as a spin-1 object, and produced an S matrix S_{LJ} but without the nondiagonal terms that would correspond to a tensor interaction. We applied the J-weighting algorithm, described and evaluated in Ref. [13] (see also [3]), to produce an effective spin-zero S matrix, S_L, and it is this that forms the basis of the discussion in this paper.

The bare potential was determined by inverting the S matrix S_L that was produced by FRESCO with the coupling to the breakup channels switched off.

IV. RESULTS

Figure 1 presents the effect upon $|S_L|$ (above) and arg S_L (below), of coupling to the breakup channels. The quantity arg S_L is twice the real phase shift. Examining $|S_L|$, it is evident that there is WW from low-L up to $L \sim 80$. Only for L above $L \sim 80$ does $|S_L|$ decrease as a result of the coupling to breakup channels. Such a decrease in $|S_L|$ is what would normally be expected as a result of coupling to reaction channels, including breakup channels. The decrease for high L in the present case leads to an increase in the total reaction cross section. Comparing with Fig. 2 of Ref. [3], we see that the pattern of WW for low L and decrease in $|S_L|$ (the 'right way', RW) for high L is qualitatively similar to that for ^{8}B scattering

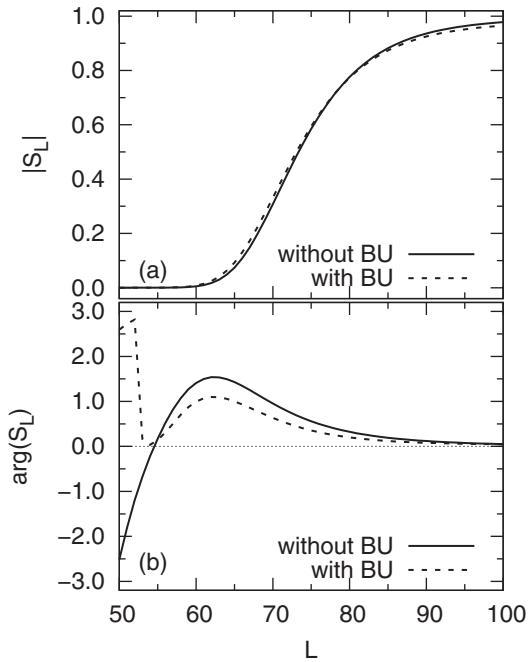

FIG. 1. For 170.3 MeV ^{8}B on ^{208}Pb, (a) $|S_L|$ and (b) arg S_L. The solid lines are for no breakup (BU) coupling and the dashed lines are for breakup coupling included. The 2π discontinuity in the lower panel reflects the principal value of arctan.

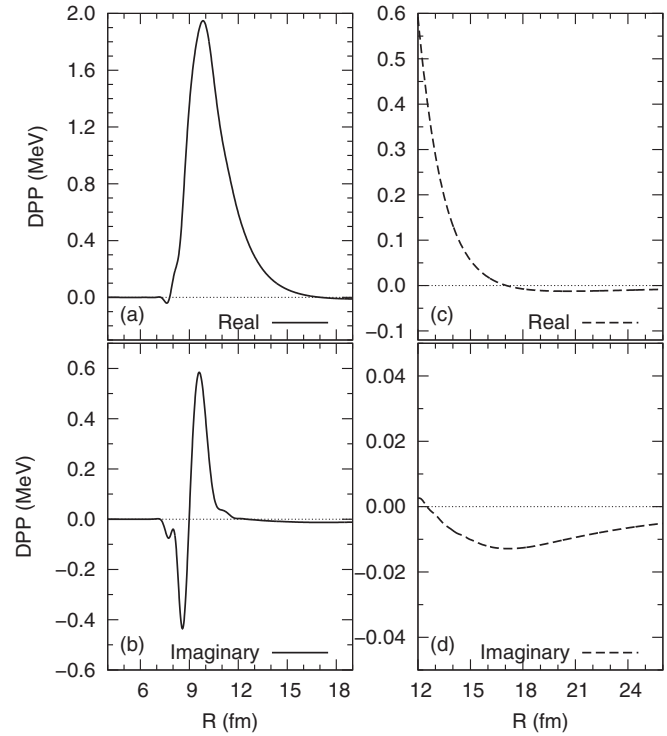

FIG. 2. For 170.3 MeV ^{8}B on ^{208}Pb, the DPP due to breakup coupling as described in the text. The real part is shown in (a) and (c) and the imaginary part in (b) and (d). The natural sign convention is used and a positive real DPP is repulsive and a positive imaginary DPP is emissive.

from ^{58}Ni at barrier energies, although here the change in $|S_L|$ is less than it is at the lower energy. Figure 1 also shows a large decrease in arg S_L due to breakup coupling. A decrease in arg S_L is generally related to a repulsive effect, and we comment on this below.

The real and imaginary DPPs due to breakup, calculated using IP inversion, are presented in Fig. 2. The strong absorption radius (SAR) evaluated using the $|S_L|^2 = \frac{1}{2}$ recipe is $\sim$ 10 fm. The real part is attractive beyond about 17 fm, and becomes strongly repulsive for smaller r, including near the SAR. The range of L-values over which arg S_L decreases, roughly $L = 55$ to $L = 80$, corresponds, for classical Coulomb orbits, to distances of closest approach between 9.0 fm and 12.5 fm. This is approximately the radial range over which the DPP is most strongly repulsive. The corresponding angular range for classical Coulomb scattering is about 20 to 28 degrees. The imaginary part has a long absorptive tail starting at about $r = 12.5$ fm but becomes emissive at smaller radii, particularly from 9 to 11 fm. The absorptive tail is responsible for the decrease in $|S_L|$ for $L > 80$. The breakup coupling thus leads to a 12 % increase in reaction cross section in spite of the WW effect for low L, as can be understood from the $2L + 1$ factor in the expression for the reaction cross section. The effect of the DPP on the angular distribution is identical to the effect of breakup that was shown in Fig. 5 of Ref. [1]. This is because the inverted potential exactly reproduces the S matrix calculated in the CDCC calculations, yielding the elastic differential cross section shown in the cited figure.

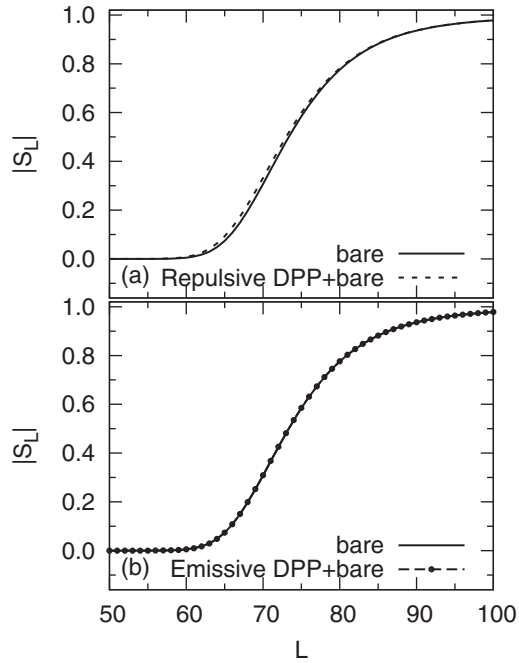

FIG. 3. For 170.3 MeV ^{8}B on ^{208}Pb, the effect on $|S_L|$ of particular contributions from the DPP added to the real, (a), and the imaginary, (b), components of the potentials, as specified in the text.

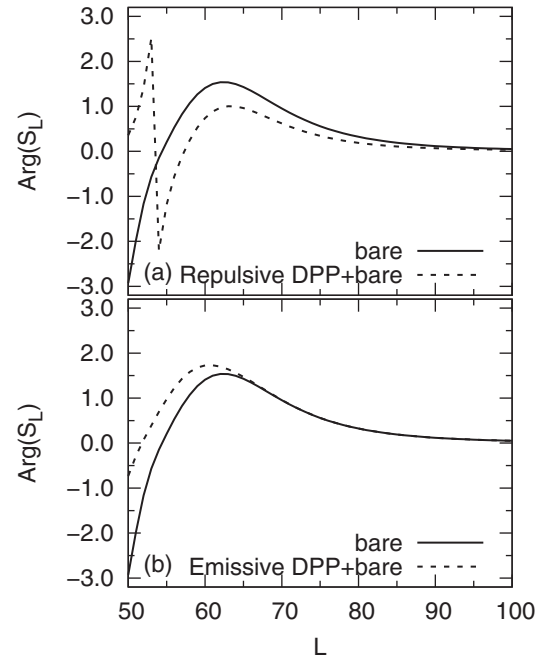

FIG. 4. For 170.3 MeV ^{8}B on ^{208}Pb, the effect on arg S_L of particular contributions from the DPP added (a) to the real and (b) to the imaginary components of the potentials, as specified in the text. The 2π discontinuity in the upper panel reflects the principal value of arctan.

Figure 3 shows the effect on $|S_L|$ of a specific part of the DPP, added as a perturbation to the bare potential. The upper panel shows the effect on $|S_L|$ of adding the repulsive part of the real component of the DPP, extending from 7.8 to 17 fm, to the real part of the bare potential. The result is a WW effect extending from low L up to $L \sim 80$, the limit of WW in the complete calculation, with no effect for higher L where, as we have seen, the tail of the imaginary DPP has its major effect. The lower panel of Fig. 3 shows the effect of adding just the emissive part of the imaginary DPP, stretching from 9 fm to 12.5 fm, to the imaginary part of the bare potential. There is a very small increase in $|S_L|$ around $L = 70$ which is not perceptible on the scale of Fig. 3. Thus, in the present case, and apart from the surface region, changes in the real potential modify $|S_L|$ but changes in the imaginary potential do not. The increase in $|S_L|$ for low-L cannot be linked to the emissive DPP.

We conclude that the WW effect is the result of the repulsive real DPP which leads to less penetration of the ^{8}B nucleus into the absorptive potential. However, this account leaves the repulsive effect itself unexplained, and the WW change in $|S_L|$ might be better understood as an effect of the coupling process that leads to repulsive potential in a local representation. The repulsive effect may itself be due to a reduced penetration of the excited projectile, in the breakup channels, into the attractive potential.

Figure 4 shows the effects upon arg S_L of adding the same specific parts of the DPP to the real and imaginary parts of the bare potential as specified above for Fig. 3. The upper panel shows the remarkably large reduction in the real phase shift resulting from the added repulsion in the real component. As an effect of repulsion on arg S_L it is completely plausible. However, it implies that the relatively small effect of breakup (or equivalently of the DPP that exactly reproduces the S_L) on the angular distribution requires comment. A similar effect was previously discussed [14] in connection with ^{6}He scattering at energies near the barrier: changes in arg S_L, and the long range real DPP, had remarkably little effect on the angular distributions. This was postulated to be a result of nearside dominance so that no interfering far-side amplitude contributes to the angular distribution. In the present case it is found that removing the attractive real DPP for $r > 17$ fm makes almost no visible change to the angular distribution. The reduction in arg S_L above $L = 55$, due to the repulsive real DPP, is not negligible and is associated with most of the observable change in the angular distribution. The predominant influence of the real part of the DPP, suggested by Figs. 3 and 4, becomes apparent in Fig. 5 which compares the effects of the real and imaginary DPPs upon the angular distribution. The solid line represents the angular distribution for the bare potential, the dotted line shows that the effect of adding the imaginary part of the DPP is barely apparent as a small reduction near the peak at 14°. Beyond the peak, the increase in angular distribution when the real part is added is almost indistinguishable from the effect of the complete DPP. The effect of the emissive imaginary component of the DPP upon arg S_L (see Fig. 4), is confined to $L <\sim 65$, and this can be seen from Fig. 5 to have a very small effect on the angular distribution.

The coupling to breakup channels results in an increase in the total reaction cross section of just 407 mb, reflected in the reduction in $|S_L|$ for $L > 80$. This is much less than the cross section to the breakup channels, which is 707 mb. The cross

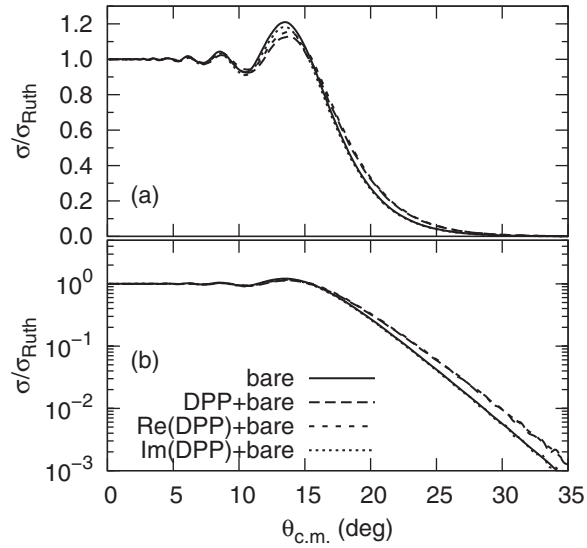

FIG. 5. Angular distributions for 170.3 MeV ^{8}B on ^{208}Pb, comparing the effects of the real and imaginary components of the DPP, are presented as a ratio to the Rutherford cross section. The linear plot (a) and logarithmic plot (b) reveal different aspects of the effects. In each panel, the solid line is for the bare potential, the long dashes are for the complete DPP, the short dashes are for the real part added to the bare potential and the dotted line is for the imaginary part added to the bare potential.

section to all other channels, presumably including fusion, must therefore be reduced by coupling to breakup channels. This is consistent with our picture in which a predominantly repulsive real DPP reduces the penetration of the projectile into the absorptive potential. At energies near the Coulomb barrier, it has been previously observed [2,5] that a large breakup cross section, associated with a relatively small effect on the angular distribution and the total reaction cross section, distinguishes the proton halo nucleus ^{8}B from other weakly bound light nuclei.

V. CONCLUSIONS AND DISCUSSION

The natural expectation is that a perturbation in the real part of a potential predominantly modifies $\arg S_L$ and a perturbation in the imaginary part predominantly modifies $|S_L|$. This expectation is fulfilled for nucleons and other weakly absorbed particles [15] and also, as we have seen, for ^{8}B for high L partial waves. But contrary to this, it is changes in the real potential that modify $|S_L|$ for ^{8}B away from the far surface. This corresponds to our demonstration that the WW effect follows from the appearance of a repulsive real DPP. It is this DPP that can be understood to repel the projectile from the absorptive region. In this work we have shown that a specific pattern of WW and RW, that applied to ^{8}B scattering near the Coulomb barrier, persists to energies that are about three times higher with respect to the Coulomb barrier, corresponding to an almost seven times higher laboratory energy. This pattern was distinctly different from that found for other halo and weakly bound nuclei [3] which exhibited WW over a wider range of L values. There were other respects [2] in which the scattering of ^{8}B differed from the other cases studied, and it tempting to ascribe this to ^{8}B being a proton-halo nucleus. It would be interesting to learn whether the more general difference between ^{8}B and other light weakly bound nuclei [2], persist to high energies, perhaps as a characteristic of proton halo nuclei.

The coupling to the breakup channels results in an increase in the total reaction cross section that is much less than the cross section to the breakup channels. It follows that the cross section to all other channels, presumably including fusion, must be reduced. This corresponds to the WW effect for low-L and can be seen as a consequence of the repulsive DPP.

The complex DPP of Fig. 2, when added to the bare potential, precisely reproduces the elastic scattering calculated with the inclusion of breakup processes, as specified in Sec. II. However, this total potential does not provide a unique description of the elastic scattering, since the DPP of Fig. 2 is a local and L-independent representation of nonlocal and explicitly L-dependent processes [16–18]. Concerning nonlocality, note that the well-known arguments [19] for the short range of nonlocalities for composite particles apply to the folding of exchange non-locality, not to dynamic nonlocalities [16–18]. For a discussion of L dependence, see Ref. [20].

The results that we have presented here arise from a rather simple model of ^{8}B and its breakup; it would be worthwhile to confirm that the general nature of the results are confirmed with a more realistic model. Presumably the multipole strengths and energy transfers are the key determinants.

ACKNOWLEDGMENTS

This work is supported by the the National Natural Science Foundation of China under Grants No. 11275018, 11021504, and 11035001.

[1] Y. Y. Yang *et al.*, Phys. Rev. C **87**, 044613 (2013).
[2] E. F. Aguilera *et al.*, Phys. Rev. C **79**, 021601(R) (2009).
[3] N. Keeley, R. S. Mackintosh, and C. Beck, Nucl. Phys. A **834**, 792c (2010).
[4] R. S. Mackintosh and D. Y. Pang, Phys. Rev. C **86**, 047602 (2012).
[5] R. S. Mackintosh (unpublished).
[6] N. Austern, Y. Iseri, M. Kamimura, M. Kawai, G. Rawitscher, and M. Yahiro, Phys. Rep. **154**, 125 (1987).
[7] I. J. Thompson, Comput. Phys. Rep. **7**, 167 (1988).
[8] A. J. Koning and J. P. Delaroche, Nucl. Phys. A **713**, 231 (2003).
[9] Y. P. Xu and D. Y. Pang, Phys. Rev. C **87**, 044605 (2013).
[10] V. I. Kukulin and R. S. Mackintosh, J. Phys. G: Nucl. Part. Phys. **30**, R1 (2004).
[11] R. S. Mackintosh, arXiv:1205.0468 (2012).
[12] R. S. Mackintosh, Scholarpedia **7**, 12032 (2012).
[13] N. Keeley and R. S. Mackintosh, Phys. Rev. C **77**, 054603 (2008).

[14] R. S. Mackintosh and N. Keeley, Phys. Rev. C **79**, 014611 (2009).
[15] R. S. Mackintosh and A. M. Kobos, J. Phys. G: Nucl. Part. Phys. **5**, 359 (1979).
[16] H. Feshbach, Ann. Phys. (NY) **5**, 357 (1958); **19**, 287 (1962).
[17] G. R. Satchler, *Direct Nuclear Reactions* (Clarendon Press, Oxford, 1983).
[18] G. H. Rawitscher, Nucl. Phys. A **475**, 519 (1987).
[19] D. F. Jackson and R. C. Johnson, Phys. Lett. B **49**, 249 (1974).
[20] R. S. Mackintosh, arXiv:1302.1097 (2013).